J Mater Sci (2021) 56:6945–6954

Energy materials

Improving hydrogen evolution activity of two-dimensional nanosheets $MoNi_4/MoO_{2.5}$-NF self-supporting electrocatalyst by electrochemical-cycling activation

Gang Yan[1,*], Yefan Gu[1], Alateng Shaga[1,*], Kun Wang[1], Lijie Zhan[1], and Zhongmou Liu[2,*]

[1] *College of Material Science and Engineering, Jilin Jianzhu University, Changchun 130118, China*
[2] *Key Laboratory of Songliao Aquatic Environment, Ministry of Education, Jilin Jianzhu University, Changchun, China*

Received: 30 October 2020
Accepted: 14 December 2020

ABSTRACT

Alloys, especially Mo–Ni alloys, are excellent HER electrocatalysts in alkaline solution. The HER activity of the Mo–Ni alloys can be improved by grafting H_2O dissociation promoters (metal oxides or hydroxides) to promote the dissociation of H_2O in alkaline solution. However, most of the reported Mo–Ni alloys grafting with H_2O dissociation promoters only have simple one-dimensional (1D) structures, which cannot further improve the catalytic performance. Compared with 1D nanomaterials, two-dimensional (2D) nanomaterials have higher specific surface area, electrical conductivity, more exposed active sites and mass transfer channels. Herein, a novel 2D nanosheets self-supporting composite electrocatalyst $MoNi_4/MoO_{2.5}$-NF derived from the $NiMoO_4$ nanosheets was reported for the first time. Benefiting from the unique 2D nanosheets structure and the synergistic effect of each component, the catalyst shows high electrocatalytic HER activity in 1 M KOH solution. The $MoNi_4/MoO_{2.5}$-NF needs overpotential of 49 mV to reach 10 mA cm^{-2}. The HER activity of $MoNi_4/MoO_{2.5}$-NF can be further improved through electrochemical-cycling activation (CV) process. After 10 CV cycles, the overpotential to reach 10 mA cm^{-2} of the catalyst decreased from 49 to 27 mV and even exceeded 20% Pt/C (32 mV). The improvement of HER performance is attributed to the increase in the electrochemically active surface area, the reduced impedance and Tafel slope after CV process.

Handling Editor: Kyle Brinkman.

Address correspondence to E-mail: yang431@nenu.edu.cn; altsg@jlju.edu.cn; liuzm6988@163.com

https://doi.org/10.1007/s10853-020-05698-w

GRAPHICAL ABSTRACT

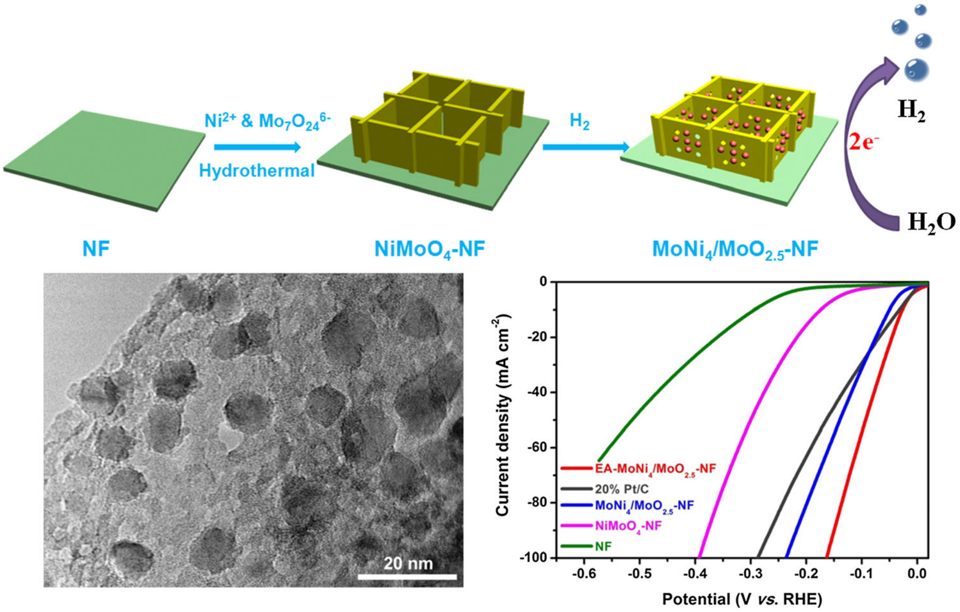

Introduction

With the urgent need of energy demand and the gradual depletion of non-renewable energy, people are committed to looking for benign, sustainable, ecological friendly energy to replace the exhausted fossil fuel [1, 2]. H_2 is a clean energy and ideal energy carrier. Among various production methods, the alkaline water electrolysis technology has been proved to be a promising technique [3, 4]. The advantages of the alkaline water electrolysis technology include that the availability of raw water is relatively unlimited and can be easily obtained. In addition, a large amount of high-purity H_2 can be obtained by this method [5]. Noble metal Pt is the most efficient hydrogen evolution catalyst, but the high price makes it necessary to explore cheap non-noble metal hydrogen evolution catalyst.

At present, a variety of transition metal-based HER catalysts, including alloys [6–9], carbides, [10–13] phosphides, [14–17] nitrides, [18–21] sulfides [22, 23] and borides [24–27] have been proved to be possible to replace Pt. Among them, alloys, especially Mo–Ni alloys, are excellent HER catalysts in alkaline electrolyte. This is because Mo–Ni alloys have a Pt-like adjustable electron density state, which can promote the adsorption and desorption process of H_{ads} [28, 29]. However, the Mo–Ni alloys catalysts still have some problems, such as high hydrogen evolution overpotential and sluggish reaction kinetics (high Tafel slope) in alkaline solution, which makes it still unable to replace Pt. In recent years, the grafting of H_2O dissociation promoters (metal oxides or hydroxides) onto the surface of Pt or transition metal HER catalysts can promote the dissociation of H_2O, thus accelerating the slow kinetics of Volmer reaction in alkaline solutions [30, 31]. Recent studies show that the combination of Mo–Ni alloys with metal oxide (MoO_x) can effectively accelerate the Volmer reaction kinetics and improve the catalytic activity. However, most of the reported Mo–Ni alloys grafting with metal oxide only have simple one-dimensional (1D) structures, such as cuboids, [32] nanowires [33] and nanorods, [34] which cannot further improve the HER performance. Compared with 1D nanomaterial, two-dimensional (2D) nanomaterials have higher specific surface area, electrical conductivity, more exposed active sites and mass transfer channels, which make them attract extensive attention in the field of electrocatalysis [35]. If the composite with two-dimensional nanosheet structure can be prepared, it is expected to further improve the catalytic activity. However, how to integrate various active components (Mo–Ni alloys and metal oxides) into 2D nanosheets structure is a big challenge.

Herein, a novel 2D nanosheets self-supporting composite electrocatalyst $MoNi_4/MoO_{2.5}$-NF was reported for the first time. This self-supporting catalyst is composed of $MoO_{2.5}$ nanosheets arrays embedded with $MoNi_4$ alloy nanoparticles. Benefiting from the 2D nanosheets structure and synergistic effect of the components, this electrocatalyst shows high HER activity in alkaline solution. In 1 M KOH solution, the $MoNi_4/MoO_{2.5}$-NF needs overpotential of 49 mV to reach 10 mA cm^{-2}. The HER activity of $MoNi_4/MoO_{2.5}$-NF can be further improved through electrochemical-cycling activation (CV) process. After 10 CV cycles, the overpotential to reach 10 mA cm^{-2} of the activated catalyst (EA-$MoNi_4/MoO_{2.5}$-NF) decreased from 49 to 27 mV and even exceeded 20% Pt/C (32 mV). The improvement of HER performance was attributed to the increase in the electrochemically active surface area (ECSA) and the decreased impedance and Tafel slope after CV process.

Results and discussion

The preparation process of the $MoNi_4/MoO_{2.5}$-NF electrocatalyst is shown in Scheme 1 and supplementary information. The first step is to grow the 2D $NiMoO_4$ nanosheets arrays precursor on Ni foam by hydrothermal method. After the precursor was reduced in H_2, the 2D $MoO_{2.5}$ nanosheets embedded with $MoNi_4$ alloy nanoparticles can be obtained. The XRD patterns of precursor and reduction product are shown in Fig. 1. As shown in Fig. 1a, the diffraction peaks at 14.2°, 19.0°, 23.8°, 25.4°, 28.9°, 32.6°, 39.1°, 41.1°, 43.8°, 47.3° and 53.4° correspond to the (110), (101), (− 121), (− 112), (220), (022), (− 402), (400), (330), (− 204) and (− 510) planes of the $NiMoO_4$ phase (JCPDS card no. 33–0948), respectively. The XRD patterns of the reduction product are shown in Fig. 1b, which match well with the $MoNi_4$ (JCPDS card no. 65–5480). Except for the XRD patterns of the $MoNi_4$, no other diffraction peaks can be observed, which indicated that the Mo–O species in the reduction products may exist in amorphous state. The surface chemical states of oxide precursors $NiMoO_4$-NF and the reduction products $MoNi_4/MoO_{2.5}$-NF were further studied by XPS. The survey XPS shows that the catalyst contained Ni, Mo and O elements (Fig. S1). Figure 1c shows the HR-XPS spectra of Ni 2p before and after H_2 reduction. The oxide precursor $NiMoO_4$-NF only shows Ni^{2+} signal (857.1 eV). After H_2 reduction, the reduction product $MoNi_4/MoO_{2.5}$-NF shows a strong Ni^0 signal (854.2 eV) and a weak Ni^{2+} signal. The results show that the Ni^{2+} in precursor oxide are almost completely reduced to Ni^0 after hydrogen reduction, and a small amount of Ni^{2+} belongs to the surface oxidized Ni species in contact with air. Figure 1d shows the HR-XPS spectra of Mo 3d before and after H_2 reduction. Only Mo^{6+} signal (232.0 eV) can be found in the precursors $NiMoO_4$-NF. After H_2 reduction, Mo with low valence of Mo^{4+} (230.5 eV, 229.0 eV) and Mo^0 (226.1 eV) can be observed. Combined with the XRD results, the Mo^0 signal should be related to the $MoNi_4$ alloy. The Mo^{6+} signal can still be observed in the reduction products, and the ratio of

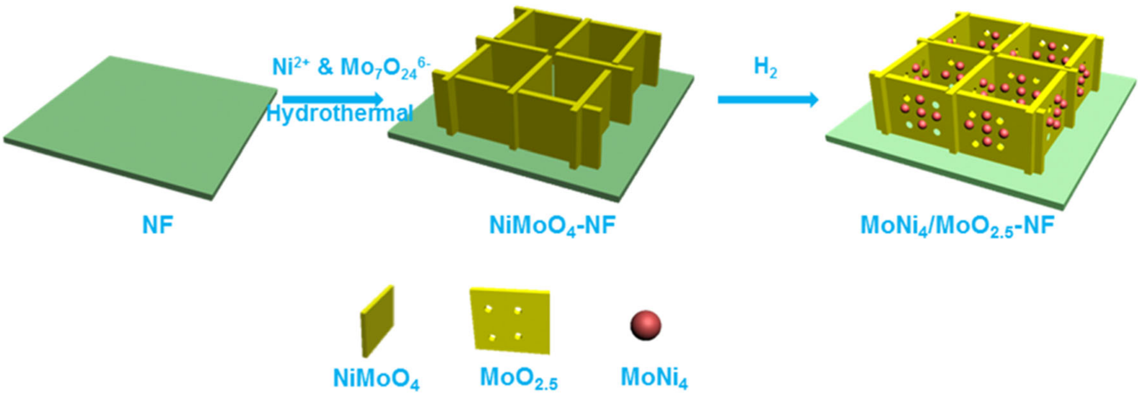

Scheme 1 Synthetic process of $MoNi_4/MoO_{2.5}$-NF electrocatalyst.

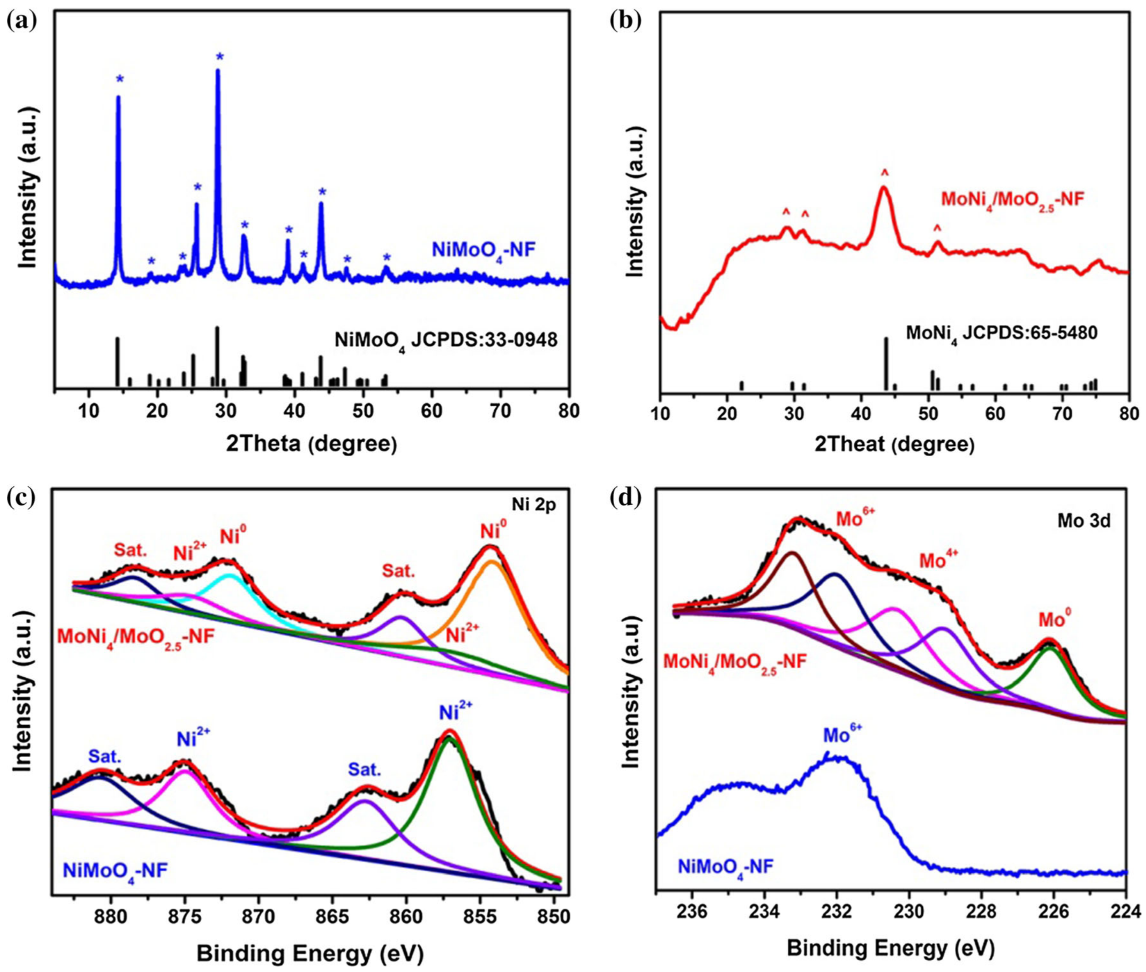

Figure 1 XRD patterns of **a** $NiMoO_4$-NF; **b** $MoNi_4/MoO_{2.5}$-NF; HR-XPS spectra of **c** Ni 2p and **d** Mo 3d.

Mo^{6+}: Mo^{4+} is about 1:1. The XPS results show that after hydrogen reduction, almost all of the Ni^{2+} species is reduced to Ni^0 ($MoNi_4$ alloy), while Mo^{6+} species is only partially reduced, part of which is reduced to Mo^0 ($MoNi_4$ alloy), the other part is reduced to low valence oxide Mo^{4+}, and some Mo^{6+} still exists in the highest valence state.

The SEM image of NF shows that the surface is very smooth and there are micron-sized pores in the NF framework (Fig. 2a). Figure 2b shows that the ultrathin $NiMoO_4$ nanosheets arrays are grown on the NF and the spacing between the nanosheets is about 200 nm. The SEM image of hydrogen reduction products $MoNi_4/MoO_{2.5}$-NF is shown in Fig. 2c. After hydrogen reduction, the material still maintains the nanosheet structure, but the surface of the nanosheet becomes rough obviously. The TEM image of hydrogenated reduction product shows that the $MoNi_4$ nanoparticles with a size of about 8 nm are evenly distributed on the $MoO_{2.5}$ nanosheets (Fig. S2). In addition, hydrogenated holes with diameter about 4 nm can be observed on the nanosheets (Fig. 2d). The HRTEM image of hydrogenated reduction products shows that the lattice spacing of diffraction fringes is 0.21 nm, corresponding to (121) crystal plane of $MoNi_4$ (Fig. 2e). No other lattice diffraction fringes were observed except for the $MoNi_4$ nanoparticles. This result is consistent with the XRD results, which indicate that the hydrogen-reduced nanosheets exist as amorphous Mo–O species with low valence. Since the XPS result shows that the ratio of Mo^{6+} to Mo^{4+} is 1:1, the chemical formula of the nanosheets after hydrogen reduction can be determined as $MoO_{2.5}$. The EDS mapping images of $MoNi_4/MoO_{2.5}$-NF are shown in Fig. 2f–i. Ni, Mo and O elements can be observed. The BET surface area of the $MoNi_4/MoO_{2.5}$-NF is 40 m^2/g (Fig. 3a). The pore size distribution of the

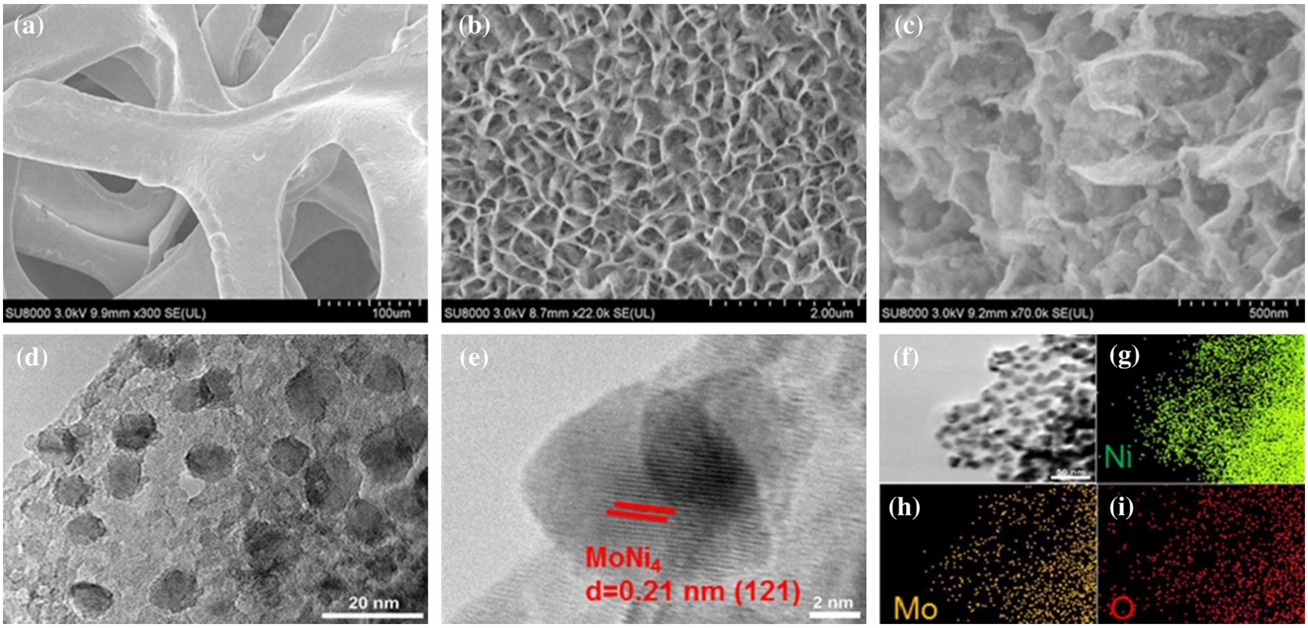

Figure 2 SEM image of **a** NF; **b** $NiMoO_4$-NF; **c** $MoNi_4/MoO_{2.5}$-NF; **d**–**e** TEM and HRTEM image of $MoNi_4/MoO_{2.5}$-NF; **f**–**i** EDAX elemental mapping of $MoNi_4/MoO_{2.5}$-NF.

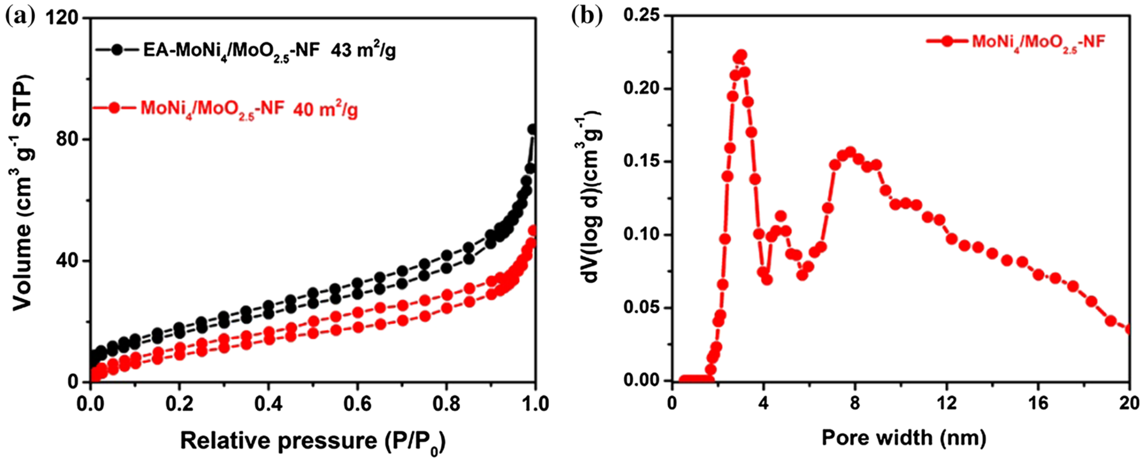

Figure 3 The BET surface area (**a**) and pore size distribution (**b**).

$MoNi_4/MoO_{2.5}$-NF is between 3 and 10 nm (Fig. 3b). These nanopores mainly belong to the pores on the nanosheets caused by hydrogenation.

The electrocatalytic HER performances of $MoNi_4/MoO_{2.5}$-NF and control samples are studied in 1.0 M KOH solution. The LSV curves of samples are shown in Fig. 4a. The HER activity of NF and $NiMoO_4$-NF is very poor, which require high overpotential of 295 mV and 173 mV to reach the current density of 10 mA cm^{-2}. The hydrogenated product $MoNi_4/MoO_{2.5}$-NF displays superior HER activity compared to that of $NiMoO_4$-NF, which only requires a very low overpotential of 49 mV to reach the same current density. The HER activity of $MoNi_4/MoO_{2.5}$-NF can be further improved through electrochemical-cycling activation (CV) process. After 10 CV cycles, the overpotential to reach 10 mA cm^{-2} of the catalyst (EA-$MoNi_4/MoO_{2.5}$-NF) decreased from 49 to 27 mV and even exceeded that of 20% Pt/C (32 mV). This electrochemical activation has been widely reported and proved to be an effective strategy to enhance the activity of catalysts [36–39]. The Tafel slopes are tested to study the reaction kinetics of samples. As shown in Fig. 4b, the Tafel slopes of $NiMoO_4$-NF and

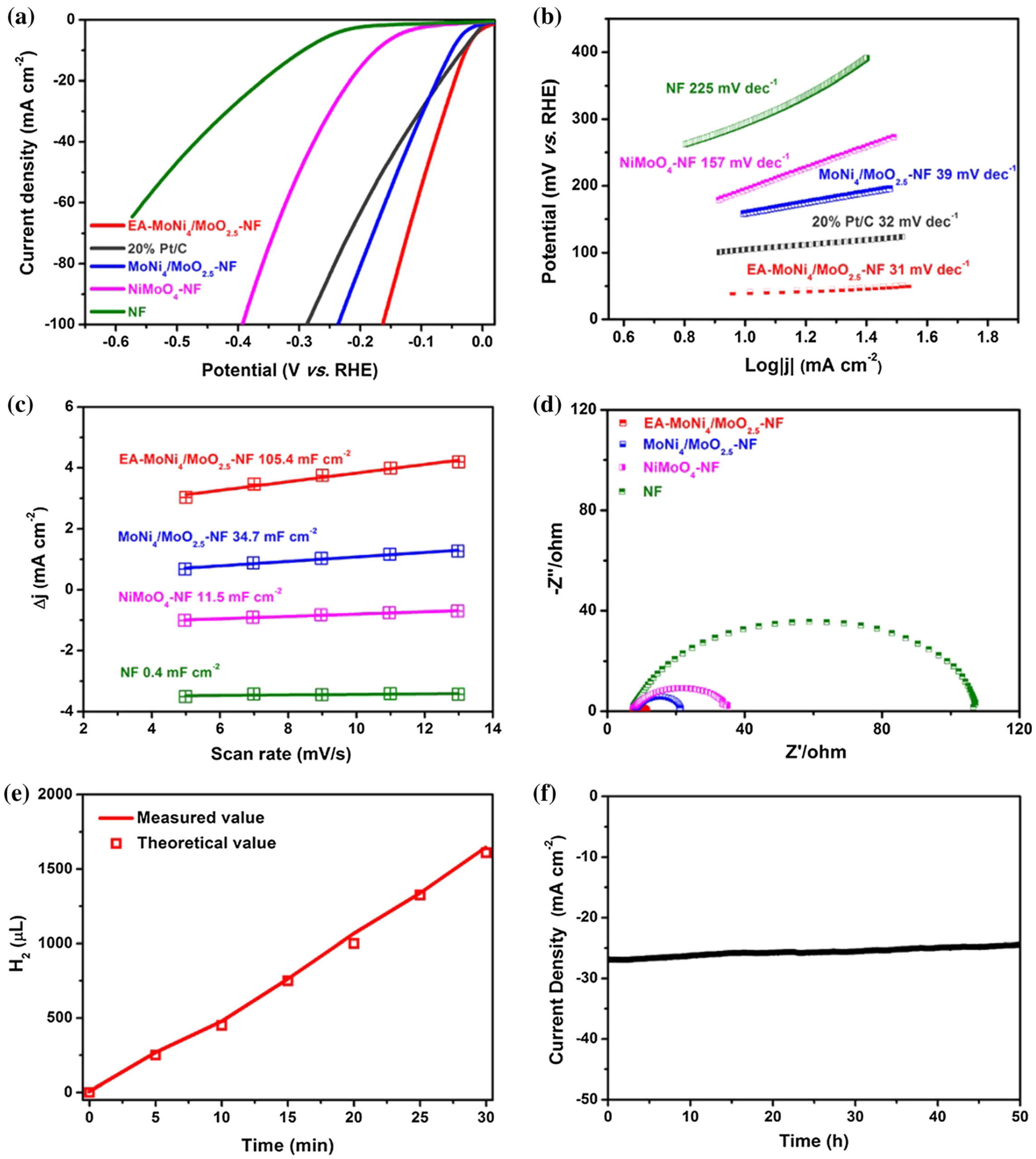

Figure 4 The HER performance of $MoNi_4/MoO_{2.5}$-NF and control samples in 1 M KOH. **a** LSV curves, **b** Tafel plots, **c** capacitive currents density as a function of scan rate, **d** EIS Nyquist plots, **e** Faradaic efficiency at different overpotentials, **f** Chronopotentiometry curves.

NF are 157 mV dec^{-1} and 225 mV dec^{-1}, respectively, indicating their very sluggish HER reaction kinetics. The Tafel slope of $MoNi_4/MoO_{2.5}$-NF is 39 mV dec^{-1}. This Tafel slope value indicates that the rate-determining step of $MoNi_4/MoO_{2.5}$-NF was Tafel reaction, which can be related to the acceleration of sluggish Volmer reaction by the $MoO_{2.5}$. After CV activation, the Tafel slope of the EA-$MoNi_4/MoO_{2.5}$-NF drops to 31 mV dec^{-1}, even lower than that of 20% Pt/C (32 mV dec^{-1}). This result indicates that the EA-$MoNi_4/MoO_{2.5}$-NF has more favorable HER reaction kinetics than that of the $MoNi_4/MoO_{2.5}$-NF. The double-layer capacitances (C_{dl}) of samples are tested by CV measurements. As shown in Fig. 4c, the C_{dl} of $NiMoO_4$-NF and NF is 11.5 mF cm^{-2} and 0.4 mF cm^{-2}, respectively, indicating their very low electrochemically active surface area (ECSA). The C_{dl} of $MoNi_4/MoO_{2.5}$-NF is

34.7 mF cm^{-2}, which is significantly higher than that of $NiMoO_4$-NF. After CV activation, the C_{dl} of the EA-$MoNi_4/MoO_{2.5}$-NF is increased dramatically to 105.4 mF cm^{-2}. This result indicates that electrochemical activation can effectively increase the electrochemically active surface area of the catalyst and improve the electrocatalytic performance. The electrochemical impedance spectroscopy (EIS) of samples are tested to study the HER process kinetics. As shown in Fig. 4d, the charge transfer resistance (R_{ct}) of EA-$MoNi_4/MoO_{2.5}$-NF, $MoNi_4/MoO_{2.5}$-NF, $NiMoO_4$-NF and NF is 4, 13, 26 and 83 Ω, respectively. The EA-$MoNi_4/MoO_{2.5}$-NF has the smallest R_{ct}, which shows rapid electron transport and HER kinetics. This result indicates that electrochemical activation can effectively reduce the impedance of the catalyst and improve the electrocatalytic performance. The electrocatalytic Faraday efficiency of EA-$MoNi_4/MoO_{2.5}$-NF is nearly 100% (Fig. 4e), which indicates that the electron utilization efficiency is very high and no other side reactions occur. The chronoamperometry test shows that the catalyst can maintain high efficiency and stable electrolysis for at least 50 h (Fig. 4f). Compared with the one-dimensional electrocatalytic materials with similar composition (i.e., Mo–O species and Ni–Mo alloy complexes) previously reported, these two-dimensional layered electrocatalysts reported here show better electrocatalytic properties. The comparison of electrocatalytic performance between the 2D nanosheets $MoNi_4/MoO_{2.5}$-NF and the 1D composite catalysts (composed of alloy and metal oxide/hydroxide) is shown in Table S1.

In order to further explore the reason for the improvement of the performance of the catalyst after electrochemical activation, the XRD, SEM, TEM and BET of the $MoNi_4/MoO_{2.5}$-NF before and after the electrochemical activation were characterized. The XRD diffraction patterns of $MoNi_4/MoO_{2.5}$-NF before and after the electrochemical activation are shown in Fig. 5a. The XRD patterns of the EA-$MoNi_4/MoO_{2.5}$-NF sample match well with the $MoNi_4$ phase. The SEM and TEM images of the EA-$MoNi_4/MoO_{2.5}$-NF also show no change compared with that of $MoNi_4/MoO_{2.5}$-NF (Fig. 5b,c). The BET specific surface area of the EA-$MoNi_4/MoO_{2.5}$-NF is 43 m^2/g, which is similar to the $MoNi_4/MoO_{2.5}$-NF (40 m^2/g, Fig. 3a). In addition, the double-layer capacitances (C_{dl}), Tafel slope and charge transfer resistances (Rct) of EA-$MoNi_4/MoO_{2.5}$-NF are significantly higher than that of the $MoNi_4/MoO_{2.5}$-NF (Fig. 4b,d). Therefore, the reason for the improvement of the HER performance of the catalyst after electrochemical activation can be associated with the enhanced electrochemically active surface area (ECSA), the decreased Tafel slope and charge transfer resistance (R_{ct}).

The bubble adhesion force and contact angle between bubbles and the catalyst surface have important effects on the release of H_2 from the catalyst surface and the promotion of the HER reaction. As shown in Fig. 5d, the bubble adhesion force and contact angle of NF are 24 μN and 128.4°. As a result, the bubbles formed on the electrode are pinned on the electrode, which is difficult to escape in the process of electrocatalysis. These bubbles will occupy the catalytic active sites and hinder the further development of hydrogen evolution reaction. The bubble adhesion force and contact angle of EA-$MoNi_4/MoO_{2.5}$-NF are 0.6 μN and 155° (Fig. 5e). The $MoNi_4/MoO_{2.5}$ nanosheet arrays reduce continuance of the three-phase lines and the area of contact between electrocatalyst and bubbles, resulting in aerophobic feature of EA-$MoNi_4/MoO_{2.5}$-NF electrodes. The nanosheet arrays structure endows the electrocatalyst a superaerophobic feature (Fig. 5f).

In conclusion, a novel 2D layered self-supporting composite electrocatalyst $MoNi_4/MoO_{2.5}$-NF was reported for the first time. Compared with the one-dimensional electrocatalytic materials with similar composition (i.e., Mo–O species and Ni–Mo alloy complexes) previously reported, this 2D nanosheets electrocatalyst reported here shows better electrocatalytic properties. The reason for the high catalytic activity of EA-$MoNi_4/MoO_{3\text{-}x}$/NiCo@NF is revealed. (1) The superior 2D nanosheets morphology and structure endow the catalyst with high specific surface area, electrical conductivity, more exposed active sites and mass transfer channels; (2) The synergistic effect between metal oxides and alloys. The $MoO_{2.5}$ can effectively promote the cleavage of H–OH bond and formed H_{ads}. The H_{ads} adsorbed on the $MoNi_4$ particles combines rapidly to release H_2. The synergistic effect of $MoO_{2.5}$ and $MoNi_4$ particles greatly reduces the overpotential and Tafel slope of HER process. (3) The electrochemical-cycling activation (CV) process can further improve the HER activity. After 10 CV cycles, the HER electrocatalytic properties even exceeded that of 20% Pt/C. This study

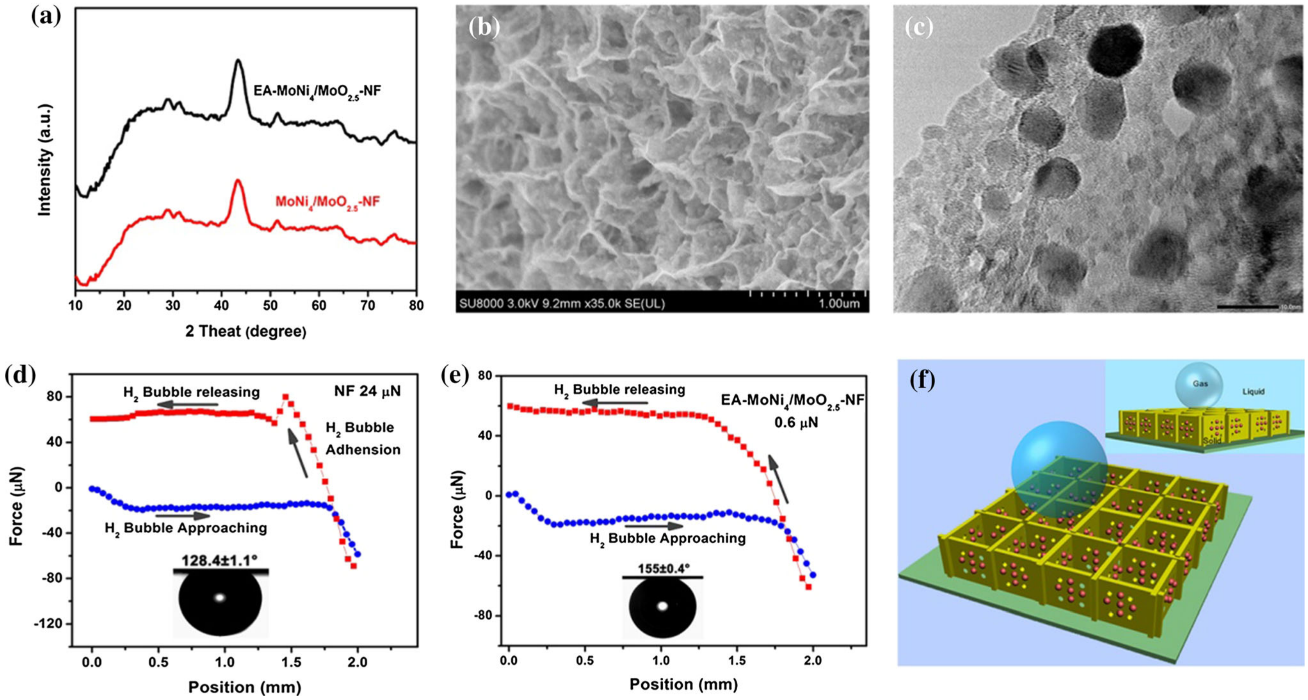

Figure 5 The XRD (**a**), SEM (**b**) and TEM (**c**) images of $MoNi_4/MoO_{2.5}$-NF before and after the electrochemical activation; **d** and **e** the bubble adhesion force and contact angles of NF and $MoNi_4/MoO_{2.5}$-NF, **f** the bubbles adhesion behaviors diagram. Inset: sectional views of the discontinuous three-phase contact line (TPLC) on $MoNi_4/MoO_{2.5}$-NF.

provides a reference for the design and synthesis of alkaline electrocatalysts to replace Pt in the future.

Acknowledgements

We acknowledge financial support from the National Natural Science Foundation of China (No. 51801070, 51808253), Natural Science Foundation of Jilin Province (No. 20200201051JC) and 13nd 5-year Science and Technology Research Program of the Department of Education of Jilin Province (No. JJKH20190858KJ). The project is supported financially by the Opening Project of Key Laboratory of Polyoxometalate Science of Ministry of Education.

Compliance with ethical standards

Conflict of interest The authors declare that they have no conflict of interest.

Supplementary information: The online version contains supplementary material available at (https://doi.org/10.1007/s10853-020-05698-w).

References

[1] Merki D, Hu XL (2011) Recent developments of molybdenum and tungsten sulfides as hydrogen evolution catalysts. Energy Environ Sci 4(10):3878–3888

[2] Wang GN, Chen TT, Gómez-García-Garcia CJ, Zhang F, Zhang MY, Ma HY, Pang HJ, Wang XM, Tan LC (2020) A high-capacity negative electrode for asymmetric supercapacitors based on a PMo_{12} coordination polymer with novel water-assisted proton channels. J Power Sour 16(29):2001626

[3] Ram S, Dusan T, Nenad M (2011) Enhancing hydrogen evolution activity in water splitting by tailoring Li^+-$Ni(OH)_2$-Pt interfaces. Science 334(6060):1256–1260

[4] Li YG, Wang HL, Xie LM (2011) MoS_2 nanoparticles grown on graphene: an advanced catalyst for the hydrogen evolution reaction. J Am Chem Soc 133(19):7296–7299

[5] Wang MY, Wang Z, Gong XZ (2014) The intensification technologies to water electrolysis for hydrogen production: a review. Renew Sustain Energy Rev 29:573–588

[6] Fu L, Li Y, Yao N, Yang F, Cheng G, Luo W (2020) IrMo nanocatalysts for efficient alkaline hydrogen electrocatalysis. ACS Catalysis 10(13):7322–7327

[7] Khalid M, Honorato AMB, Tremiliosi FG, Varela H (2020) Trifunctional catalytic activities of trimetallic FeCoNi alloy

nanoparticles embedded in a carbon shell for efficient overall water splitting. J Mater Chem A 8(18):9021–9031

[8] Pan QQ, Xua CY, Lia X, Zhang JF, Hu XL, Geng Y, Su ZM (2020) Porous Ni-Mo bimetallic hybrid electrocatalyst by intermolecular forces in precursors for enhanced hydrogen generation. Chem Eng J 405:126962

[9] Nguyet NTP, Sung GK, Hyoung-Juhn K, Chanho P, Byungchan H, Seung GL (2021) Catalytic activity of Ni_3Mo surfaces for hydrogen evolution reaction: a density functional theory approach. Appl Surf Sci 537:147894

[10] Hu Y, Jensen JO, Zhang W, Cleemann LN, Xing W, Bjerrum NJ, Li Q (2014) Hollow spheres of iron carbide nanoparticles encased in graphitic layers as oxygen reduction catalysts. Angew Chem Int Ed Engl 53(14):3675–3679

[11] Shanenkov I, Ivashutenko A, Shanenkova Y, Nikitin D, Zhu Y, Li J, Han W, Sivkov A (2020) Composite material WC_{1-x}@C as a noble-metal-economic material for hydrogen evolution reaction. J Alloy Compd 834:155116

[12] Niu SS, Yang J, Qi HF, Su Y, Wang ZY, Qiu JS, Wang AQ, Zhang T (2020) Single-atom Pt promoted Mo_2C for electrochemical hydrogen evolution reaction. J Energy Chem. https://doi.org/10.1016/j.jechem.2020.08.028

[13] Hyeong MJ, Youngkwon K, Duck HY (2021) One-pot synthesis of molybdenum carbide/N-doped carbon nanotube composite using nitrilotriacetic acid for efficient hydrogen evolution. J Alloy Compd 855:157420

[14] Popczun EJ, Read CG, Roske CW, Lewis NS, Schaak RE (2014) Highly active electrocatalysis of the hydrogen evolution reaction by cobalt phosphide nanoparticles. Angew Chem 126(21):5531–5534

[15] Zhang Z, Lu B, Hao J, Yang W, Tang J (2014) FeP nanoparticles grown on graphene sheets as highly active non-precious-metal electrocatalysts for hydrogen evolution reaction. Chem Commun 50(78):11554–11557

[16] Yang BB, Xu JY, Bin D, Wang J, Zhao JZ, Liu YX, Li BX, Fang XN, Liu Y, Qiao L, Liu LF, Liu BH (2020) Amorphous phosphatized ruthenium-iron bimetallic nanoclusters with Pt-like activity for hydrogen evolution reaction. Appl Catal B 283:119583

[17] Lin Y, Zhang ML, Zhao LX, Wang LM, Cao DM, Gong YQ (2021) Ru doped bimetallic phosphide derived from 2D metal organic framework as active and robust electrocatalyst for water splitting. Appl Surf Sci 536:147952

[18] Xie J, Li S, Zhang X, Zhang J, Wang R, Zhang H, Pan B, Xie Y (2014) Atomically-thin molybdenum nitride nanosheets with exposed active surface sites for efficient hydrogen evolution. Chem Sci 5(12):4615–4620

[19] Shi J, Pu Z, Liu Q, Asiri AM, Hu J, Sun X (2015) Tungsten nitride nanorods array grown on carbon cloth as an efficient hydrogen evolution cathode at all pH values. Electrochim Acta 154:345–351

[20] Kartick CM, Mahendra Y (2021) Palladium oxide decorated transition metal nitride as efficient electrocatalyst for hydrogen evolution reaction. J Alloy Compd 855:157511

[21] Jiang HQ, Li XS, Zang SY, Zhang WL (2021) Mixed cobalt-nitrides Co_xN and Ta_2N bifunction-modified Ta_3N_5 nanosheets for enhanced photocatalytic water-splitting into hydrogen. J Alloy Compd 854:155328

[22] Peng S, Li L, Han X, Sun M, Srinivasan M, Mhaisalkar SG, Cheng F, Yan Q, Chen J, Ramakrishna S (2014) Cobalt sulfide nanosheet/graphene/carbon nanotube nanocomposites as flexible electrodes for hydrogen evolution. Angew Chem 126(46):12802–12807

[23] Hou Y, Pang HJ, Zhang L, Li BN, Xin JJ, Li KQ, Ma HY, Wang XM, Tan LC (2020) Highly dispersive bimetallic sulfides afforded by crystalline polyoxometalate-based coordination polymer precursors for efficient hydrogen evolution reaction. J Power Sour 446:227319

[24] Kadrekarac R, Patelb N, Aryaa A (2020) Understanding the role of boron and stoichiometric ratio in the catalytic performance of amorphous Co-B catalyst. Appl Surf Sci 518:146199

[25] Hong WZ, Sun SF, Kong Y, Hu YY, Chen G (2020) Ni_x-$Fe_{1-x}B$ nanoparticle self-modified nanosheets as efficient bifunctional electrocatalysts for water splitting: experiments and theories. J Mater Chem A 8(15):7360–7367

[26] Li YJ, Huang BL, Sun YJ, Luo MC, Yang Y, Qin YN, Wang L, Li CJ, Lv F, Zhang WY, Guo SJ (2018) Multimetal borides nanochains as efficient electrocatalysts for overall water splitting. Small 15(1):1804212

[27] Hyounmyung P, Eunsoo L, Lei M, Hyunkeun J, Sinisa C, Boniface PTF (2020) Canonic-like HER activity of Cr_{1-x}-Mo_xB_2 solid solution: overpowering Pt/C at high current density. Adv Mater 32(28):2000855

[28] An L, Zang X, Ma L, Guo J, Liu Q, Zhang X (2020) Graphene layer encapsulated $MoNi_4$-$NiMoO_4$ for electrocatalytic water splitting. Appl Surf Sci 504:144390

[29] Cao GX, Chen ZJ, Yin H, Gan LY, Zang MJ, Xu N, Wang P (2019) Investigation of the correlation between the phase structure and activity of Ni–Mo–O derived electrocatalysts for the hydrogen evolution reaction. J Mater Chem A 7(17):10338–10345

[30] Xu K, Cheng H, Lv HF, Wang JY, Liu LQ, Liu S, Wu XJ, Chu WS, Wu CZ, Xie Y (2018) Controllable surface reorganization engineering on cobalt phosphide nanowire arrays for efficient alkaline hydrogen evolution reaction. Adv Mater 30(1):1703322

[31] Zhang L, Amiinu IS, Ren X, Liu Z, Du G, Abdullah MA, Zheng BZ, Sun XP (2017) Surface modification of a NiS_2

nanoarray with $Ni(OH)_2$ toward superior water reduction electrocatalysis in alkaline media. Inorg Chem 56(22):13651–13654

[32] Zhang J, Wang T, Liu P, Liao ZY, Liu SH, Zhuang XD, Chen MW, Ehrenfried Z, Feng XL (2017) Efficient hydrogen production on $MoNi_4$ electrocatalysts with fast water dissociation kinetics. Nat Commun 8:15437

[33] Chen YY, Zhang Y, Zhang X, Tang T, Luo H, Niu S, Dai ZH, Wan LJ, Hu JS (2017) Self-templated fabrication of $MoNi_4/MoO_{3-x}$ nanorod arrays with dual active components for highly efficient hydrogen evolution. Adv Mater 29(39):1703311

[34] Meng LS, Li LP, Wang JH, Fu SX, Zhang YL, Li J, Xue CL, Wei YH, Li GS (2020) Valence-engineered $MoNi_4/MoO_x$@NF as a Bi-functional electrocatalyst compelling for urea-assisted water splitting reaction. Electrochim Acta 350:136382

[35] Tan CL, Cao XH, Wu XJ, He QY, Yang J, Zhang X, Chen JZ, Zhao W, Han SK, Gwang-Hyeon N, Melinda S, Zhang H (2017) Recent advances in ultrathin two-dimensional nanomaterials. Chem Rev 117(9):6225–6331

[36] Yang C, Gao MY, Zhang QB, Zeng JR, Li XT, Abbott AP (2017) In-situ activation of self-supported 3D hierarchically porous Ni_3S_2 films grown on nanoporous copper as excellent pH-universal electrocatalysts for hydrogen evolution reaction. Nano energy 36:85–94

[37] Jin W, Chen JP (2018) Electrochemically activated Cu_2O/Co_3O_4 nanocomposites on defective carbon nanotubes for the hydrogen evolution reaction. New J Chem 42(24):19400–19406

[38] Kim YM, Jackson DHK, Lee D, Choi M, Kim TW, Jeong SY, Chae HJ, Kim HW, Park NJ, Chang HJ, Kuech TF, Kim HJ (2017) In situ electrochemical activation of atomic layer deposition coated MoS_2 basal planes for efficient hydrogen evolution reaction. Adv Funct Mater 27(34):1701825

[39] Jin QY, Ren BW, Li DQ, Cui H, Wang CX (2018) In situ promoting water dissociation kinetic of Co based electrocatalyst for unprecedentedly enhanced hydrogen evolution reaction in alkaline media. Nano energy 49:14–22